Insights on the Atomic and Electronic Structure of Boron Nanoribbons

Sumit Saxena* and Trevor A. Tyson†

Department of Physics, New Jersey Institute of Technology, Newark, New Jersey 07102, USA

(Received 12 March 2010; published 15 June 2010)

A study of the structural stability of boron nanoribbons is presented. Antiaromatic instabilities are found to destabilize boron nanoribbons. Our studies suggest that nanoribbons obtained from "α sheets" are more stable than those from reconstructed {1221} sheets and traditional triangular boron sheets. The stability of the nanoribbons increases with an increasing ribbon width resulting in an increased hole density (η) and, hence, an increased number of hexagonal motifs in the nanoribbon. The boron nanoribbons formed are mostly metallic; however, semiconducting structures have also been observed.

DOI: 10.1103/PhysRevLett.104.245502 PACS numbers: 81.07.Nb

Boron is a fairly complex element chemically, existing in at least 16 polymorphs [1]. It is used in a variety of important applications such as neutron absorption [2] and in high strength materials for making armors. High pressure experiments on bulk boron samples have shown the occurrence of a high pressure ionic phase [3] and low temperature superconductivity [4] with a critical temperature of 6 K at ~175 GPa. This element has been investigated both theoretically [5,6] and experimentally [7] in various forms like bulk boron, nanotubes [8], clusters and quasi planar sheets. The general perception of a monolayer boron sheet is that it occurs as a buckled sheet with a triangular lattice [9]. The reconstructed {1221} sheets of boron are known to be more stable than the idealized {1212} sheets [10]. Investigations have predicted that the two basic units of boron, hexagonal and pentagonal pyramids, may hold the key to form stable boron structures [11,12]. Recently, monolayers of boron comprised of triangular and hexagonal motifs [13], known as "α sheets," have been predicted to be energetically more stable than the flat triangular sheets. This has also successfully explained the stability of B_{80} fullerenes [14]. The formation of boron nanoribbons (BNRs) is expected to reveal interesting properties due to the edges, as also observed in graphene nanoribbons [15–17]. It is therefore important to establish and understand the stability of BNRs and to explore their properties from a fundamental perspective and for nanodevice and nanoelectronics applications.

We have investigated the structural instabilities of BNRs derived from reconstructed {1221}, triangular sheets and α sheets using *ab initio* density functional theory (DFT) calculations. The electronic structure of BNRs obtained from the α sheets is also studied. Cyclic systems with $4n\pi$ electrons that do not fit Huckel's $4n + 2$ rule for aromaticity are known as antiaromatic [18] systems. Antiaromaticity is understood to be responsible for the instability of BNRs obtained from the reconstructed {1221} sheets. Nanoribbons obtained from α sheets were found to be energetically more stable as compared to those obtained from the traditional puckered triangular sheets of boron. The stability of the nanoribbons is found to increase with increasing hole density (η) of the nanoribbons. Increasing the number of hexagonal motifs in the nanoribbon lattice is understood to induce stability with increasing width of the nanoribbons. BNRs with linear and armchair edges are investigated by cutting the α sheets. BNRs with linear edges (LBNR) are found to be metallic. However, nanoribbons with armchair edges (ABNR) are found to be metallic as well as semiconducting. The occurrence of semiconducting structures makes BNR junctions potential candidates for nanoelectronics applications.

DFT calculations have been performed using the plane-wave basis within both local density approximation (LDA) and generalized gradient approximation (GGA), as implemented in VASP [19,20]. Projector augmented wave (PAW) and ultrasoft pseudopotentials (USPP) have been used. The electron localization function (ELF) has been calculated using the formulation of Savin and Silvi [21]. The details have been discussed elsewhere [22–24]. The distance between two BNRs is taken to be 2 nm to minimize the interactions between the neighboring BNRs within the supercell approach. The K-point mesh of $1 \times 1 \times 31$ was taken to calculate the electronic structure.

The nomenclature for naming the BNRs merits a small review before we proceed any further. The BNRs are categorized by the arrangement of atoms and hence the width of the nanoribbons similar to that of the graphene nanoribbons [25]. BNRs with linear edges are named as N_zLBNR where N_z is the number of zigzag chains across the ribbon width as shown in Fig. 1(a) by including additional boron atoms across the ribbon width at the vacant sites in α sheets. For the LBNRs, the atoms at the edges have four neighbors as seen in the B_{20} double-ring structure [26]. The armchair edged BNRs are obtained by cutting α sheets along cells containing vacant sites. Likewise the armchair edged BNRs, N_dABNR are named after the number of dimer lines N_d of additional center boron atoms across the ribbon width as shown in Fig. 1(b).

Nanoribbons of approximately the same width up to ~1 nm were constructed from the reconstructed {1221}

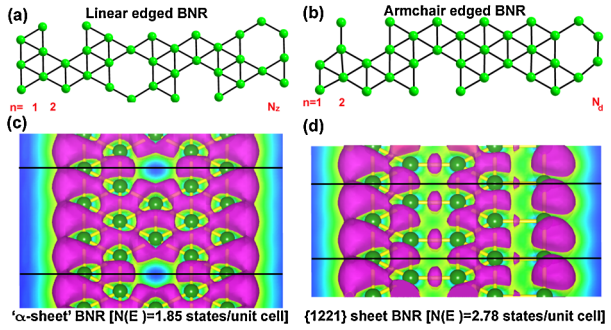

FIG. 1 (color online). Nomenclature for bare boron nanoribbons in unit cell with (a) linear and (b) armchair edges. ELF (isosurface at 0.7) for nanoribbons derived from (a) stable α sheet (b) reconstructed {1221} boron sheet. The c axis represents the ribbon axis. The unit cells are marked with black lines.

and α sheets in order to compare the stability of both the structures. We found that the nanoribbons with linear edges obtained from the α sheets are more stable with respect to those obtained from the reconstructed {1221} sheets by $\sim$0.4 eV/atom and those obtained from triangular sheets by $\sim$0.11 eV/atom. The electronic band structure and density of states showed that both the systems having linear edges are metallic. The delocalization of the π orbital from the ELF plot in Fig. 1(c) is seen to be more in nanoribbons derived from the α sheet as compared to those from the reconstructed {1221} sheets containing weaker square interlinks as seen in Fig. 1(d). This delocalization of the π orbital is understood to provide stability to the α sheets. Boron with electronic configuration of $1s^2 2s^2 p^1$ undergoes sp^2 hybridization and leaves one empty p orbital. Thus the chemical bonding of boron is electron deficient in character. This results in three center triangular BBB units to form an important constituent of boron atomic structures. The instability of reconstructed {1221} nanoribbons can be understood due to the antiaromaticity associated to the presence of triangle-square-triangle network. No dangling bonds at the edges in either of the nanoribbons are observed in the ELF plot in Figs. 1(c) and 1(d) suggesting that the linear edges in LBNRs are stable.

The stability of the BNRs is determined by the energy of formation, which is defined as $\Delta E = E_{\mathrm{BNRs}} - E_{\alpha-\mathrm{sheet}}$. The energy of formation was calculated for LBNRs of different widths having symmetric and asymmetric edges derived from the α sheets using both PAW and USPP approaches as seen in Figs. 2(a) and 2(b). It is observed that LBNRs with symmetric edges are more stable than their asymmetric counterparts. Defining the "hexagon hole density" similar to that for α sheet as

$$\eta = \frac{\text{no. of hexagon holes}}{\text{No. of atoms in unit cell of origional triangular lattice}}$$

we observe that with η approaching value of 1/9, the LBNRs with symmetric edges achieve stability as one approach an infinite α sheet. The value of $\eta = 1/9$ is important because the hexagonal sites can be most symmetrically placed in infinite α sheet. The inverse of the width also varies linearly with η. Similar trends in variation of η are observed for boron nanoribbons with asymmetric linear edges as seen in Fig. 2(b). The calculated value using GGA-PAW are in excellent agreement with previously published theoretical results [27]. The stability of the BNRs increases with increasing ribbon width and the energy of formation decreases as the inverse of the ribbon width. This can be understood due to increasing the aromaticity by increasing the number of hexagonal boron motifs in the structure. From a doping perspective, the three centered triangular motifs act as donors with a surplus of electrons in the antibonding state, while the two centered hexagonal motifs acts as acceptors thus explaining the stability with increasing width of the nanoribbon. The Bader charge [28–30] was calculated for atoms in a unit cell of α sheet. A helium atom being inert, neither attracts nor donates charge was placed inside the hole of the hexagonal motif of bare boron α sheet to determine the transfer of charge from donor to acceptor site. It was found that the charge of the He atom at acceptor site increased by $\sim$0.2 electrons while the charge on donor boron atom

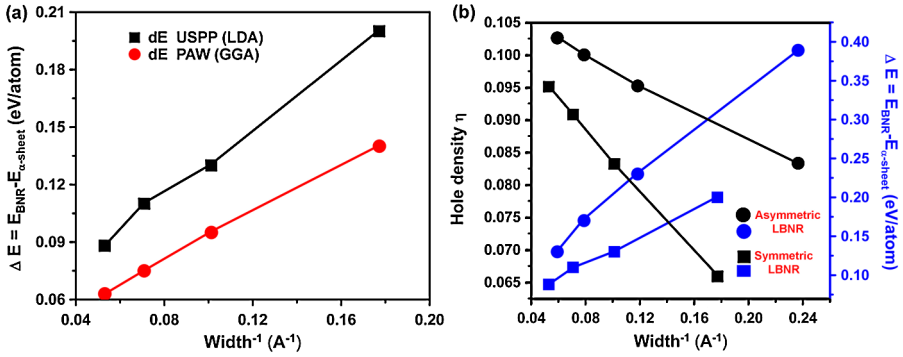

FIG. 2 (color online). (a) Variation of inverse of width with Energy of formation shows that the stability of the LBNR is inversely proportional to the width of the nanoribbon. (b) Increase in hole density (η) and stability with increasing width of the nanoribbon for LBNRs with symmetric edges represented by boxes and that for LBNRs with asymmetric edges represented by circles.

decreased by ~0.5 electrons with rest of the charge being distributed to the neighboring boron atoms on the hexagonal ring. In pure boron α sheet the ~0.5 electron charge was found to distribute on the neighboring atoms forming the hexagonal ring.

Having established the stability of nanoribbons derived from the α -sheet, we investigate the electronic and atomic structure of LBNRs and ABNRs derived from the α sheet. Each edge atom in LBNRs has four neighboring atoms as seen in Fig. 3(a) for 4LBNR. The electronic band structure and total density of states (TDOS) of 4LBNR is plotted in Fig. 3(b). Similar to boron sheets, the LBNRS are metallic with bands crossing over from conduction band to valence band across the Fermi level. A comparison of the electronic band structure plot and TDOS with 7LBNR and 10LBNR has been made in Figs. 3(c) and 3(d) respectively. Larger concentrations of the electronic bands near the Fermi level are observed with increasing width indicating increasing stability of the nanoribbons with width.

Each edge atoms on the apex in ABNR is surrounded by three neighbors while each atom at the bowl of the edge is surrounded by five atoms. This offers the possibility of edge dangling bonds and the electronic states corresponding to the edge dangling bonds in the electronic band structure diagram. Further investigation of armchair edged nanoribbons revealed the occurrence of semiconducting behavior in 7ABNR. The electronic band structure of 7ABNR in Fig. 4(b) shows the presence of indirect band gap of about 0.37 eV. It is interesting to note that this semiconducting behavior is neither observed for the narrower 4ABNR nor in wider 9ABNR nanoribbon as seen in Figs. 4(c) and 4(d) with both showing metallic character. The origin of semiconducting behavior in some structures is still not well understood and needs further investigations. Since each apex atom in the armchair edged nanoribbon has three nearest neighbors, we can add up to two Hydrogen atoms to study the contribution of the armchair edges in the band structure of boron nanoribbons [31,32]. We explore the changes in the stability and electronic properties of simplified 4ABNR by saturating each apex atom by 1H and 2H atoms. The electronic band structure diagram (Olive circles) in Fig. 4(c) shows that although 4ABNR remains metallic when saturated by 1H atom, the number of states crossing the Fermi level decreases with the modification of electronic band structure, thereby indicating the presence of edge states due to the armchair edges near the Fermi level. The optimized B-H bond length was found to be about 1.18 Å, this is very close to the $B\text{-}H_{terminal}$ bond length in Diborane [33]. However, when 2H atoms are used to saturate the armchair edges we find that a band gap opens up at the Fermi level as in Fig. 4(c) (Blue squares) indicating semiconducting behavior of the 2H saturated 4ABNR. We find that addition of one more H atoms leads to slight weakening of the B-H bond. The stability of the nanoribbons is found to decrease as the edges are saturated with increasing number of H atoms.

We have studied the structural stability and electronic properties of the boron nanoribbons derived from α sheets of boron using *ab initio* density functional theory. We find that the nanoribbons extracted from α sheets are more stable than those derived from the reconstructed {1221} boron sheets and those obtained from traditional triangular boron sheets. The stability of the nanoribbons is found to vary as an inverse of the ribbon width. The increasing presence of hexagonal motifs in boron nanoribbons increases the structural stability of the nanoribbons acting as sites for electron acceptors. Most of the nanoribbon structures are found to be metallic; however the presence of semiconducting structures is also observed.

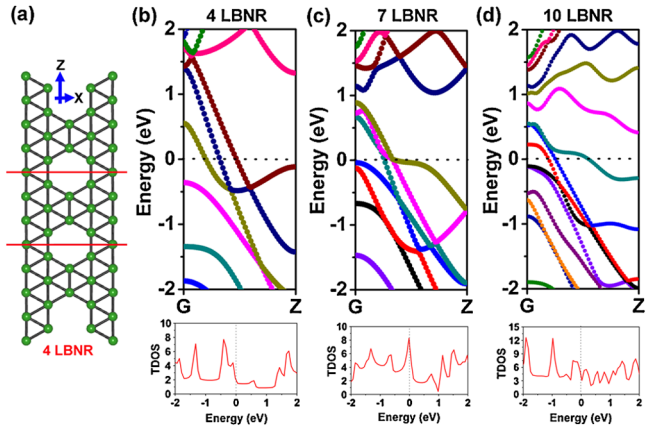

FIG. 3 (color online). (a) Atomic structure of isolated bare 4LBNR with unit cell marked by two red lines across the cross-section. The electronic band structure and the TDOS are shown for (b) 4LBNR, (c) 7LBNR, and (d) 10 LBNR. The Fermi level is adjusted to 0 eV. G is the Gamma point and the ribbon axis is along the z axis.

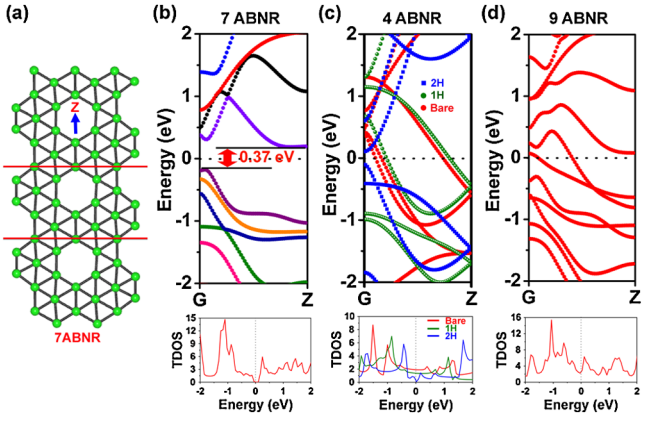

FIG. 4 (color online). (a) Atomic structure of bare 7ABNR with unit cell marked by red lines. Electronic band structure for (b) bare 7ABNR shows indirect band gap of 0.37 eV (c) bare 4ABNR and each edge atom saturated by 1H (Olive circles) and 2H atoms (Blue squares) (d) bare 9ABNR. The Fermi level is adjusted to 0 eV. G is the Gamma point and the ribbon axis is along the Z axis.

We acknowledge the computing time available to us on the NJIT University computing facility HYDRA and support from NSF DMR grant DMR-0512196.

Appendix.—The stability of the boron nanoribbons derived from the α sheet was compared to the nanoribbon structures based on triangular sheets. Flat nanoribbons formed using triangular sheets were relaxed completely. It is observed that these form one of the local minimum energy states and hence it is a metastable state. The positions of the atoms were displaced randomly by about 10% along the three coordinate axes and then relaxed; we found a lower energy structure using both USPP and PAW potentials and it remains puckered towards the center of the ribbon while it tries to flatten towards the free edges. These structures were however found to be metastable when compared to those obtained from the α sheets, with energy per atom 0.04 eV higher. In these puckered structures the atoms towards the edges release the stress by pushing the neighboring atoms away from them. This is observed as an increased puckering height of 0.93 Å as compared to 0.82 Å reported earlier for puckered infinite sheets. This tends to form flattened structure toward the ribbon edges while still maintaining the triangular lattice. The atoms at the center remain buckled as the atoms towards the center are pushed inside by atoms at both the edges.

*susax78@rediffmail.com
†Corresponding author.
tyson@adm.njit.edu

[1] J. S. Tse, Nature (London) **457**, 800 (2009).
[2] R. F. Barth, A. H. Soloway, and R. G. Fairchild, Cancer Res. **50**, 1061 (1999).
[3] A. R. Oganov *et al.*, Nature (London) **457**, 863 (2009).
[4] M. I. Eremets *et al.*, Science **293**, 272 (2001).
[5] J. Kunstmann and A. Quandt, Phys. Rev. B **74**, 035413 (2006).
[6] K. C. Lau *et al.*, Appl. Phys. Lett. **88**, 212111 (2006).
[7] D. Ciuparu *et al.*, J. Phys. Chem. B **108**, 3967 (2004).
[8] I. Boustani and A. Quandt, Europhys. Lett. **39**, 527 (1997).
[9] J. Kunstmann, A. Quandt, and I. Boustani, Nanotechnology **18**, 155703 (2007).
[10] K. C. Lau *et al.*, Chem. Phys. Lett. **418**, 549 (2006).
[11] I. Boustani, Phys. Rev. B **55**, 16426 (1997).
[12] A. Quandt, and I. Boustani, Chem. Phys. Chem. **6**, 2001 (2005).
[13] H. Tang and S. Ismail-Beigi, Phys. Rev. Lett. **99**, 115501 (2007).
[14] N. Gonzalez Szwacki, A. Sadrzadeh, and B. I. Yakobson, Phys. Rev. Lett. **98**, 166804 (2007).
[15] S. Saxena and T. A. Tyson, Carbon **48**, 1153 (2010).
[16] M. Y. Han *et al.*, Phys. Rev. Lett. **98**, 206805 (2007).
[17] L. Brey and H. A. Fertig, Phys. Rev. B **73**, 235411 (2006).
[18] R. Breslow, Acc. Chem. Res. **6**, 393 (1973).
[19] G. Kresse and D. Joubert, Phys. Rev. B **59**, 1758 (1999).
[20] G. Kresse and J. Furthmuller, Comput. Mater. Sci. **6**, 15 (1996).
[21] B. Silvi and A. Savin, Nature (London) **371**, 683 (1994).
[22] D. M. Ceperley and B. J. Alder, Phys. Rev. Lett. **45**, 566 (1980).
[23] J. P. Perdew and A. Zunger, Phys. Rev. B **23**, 5048 (1981).
[24] S. Saxena and T. A. Tyson, ACS Nano (to be published).
[25] K. Nakada *et al.*, Phys. Rev. B **54**, 17954 (1996).
[26] B. Kiran *et al.*, Proc. Natl. Acad. Sci. U.S.A. **102**, 961 (2005).
[27] Y. Ding, X. Yang, and J. Ni, Appl. Phys. Lett. **93**, 043107 (2008).
[28] G. Henkelman, A. Arnaldsson, and H. Jónsson, Comput. Mater. Sci. **36**, 354 (2006).
[29] E. Sanville *et al.*, J. Comput. Chem. **28**, 899 (2007).
[30] W. Tang *et al.*, J. Phys. Condens. Matter **21**, 084204 (2009).
[31] V. Barone, O. Hod, and G. E. Scuseria, Nano Lett. **6**, 2748 (2006).
[32] Y.-W. Son, M. L. Cohen, and S. G. Louie, Phys. Rev. Lett. **97**, 216803 (2006).
[33] S. Sakai, J. Phys. Chem. **99**, 5883 (1995).